Validation of Tank Self-Pressurization Models in Normal Gravity

Stephen Barsi and Mohammad Kassemi
National Center for Space Exploration Research
NASA Glenn Research Center *

In optimizing the design of cryogenic storage facilities for future in-orbit or on-surface applications the boil-off and the self-pressurization rates must be accurately predicted for different g-levels and for a variety of heat distributions and engineering design parameters. In this paper, a thermodynamic and a CFD model will be presented that describe the self-pressurization behavior of a flightweight partially filled LH2 experimental tank prototype in a normal gravity environment. Existing experimental data at different fill levels are used to assess the predictive capability of these models. Comparisons between the data and the model predictions indicate that the thermodynamic model can accurately predict the self-pressurization rate, but fails to capture the magnitude of the pressure rise. In contrast, the computational model captures both the self-pressurization rate and vapor pressure magnitude at lower fill levels. Slight deviations are observed for the higher fill level cases. Possible sources of this discrepancy are discussed.

Nomenclature

A	Area	$\mathbf{v}$	Velocity
β	Expansion coefficient	$\mathbf{V}$	Volume
c	Specific heat at constant volume	$\mathbf{v_s}$	Surface velocity
e	Internal energy		
k	Thermal conductivity	*Subscripts*	
L	Latent heat	B	Normal boiling point
M	Molar weight	il	Liquid side of the interface
$\dot{M}$	Mass flow rate	iv	Vapor side of the interface
μ	Dynamic viscosity	l	Liquid
$\mathbf{n}$	Normal vector	out	Vent
$\mathbf{q}$	Heat flux	s	Saturation
$\dot{Q}$	Heat power	T	Tank
p	Pressure	w	Total wall boundary
ρ	Density	wl	Wetted wall boundary
R	Gas constant	wv	Non-wetted wall boundary
T	Temperature	v	Vapor

I. Introduction

Detailed scientific and engineering work are needed in order for NASA to optimize the performance of its cryogenic storage tank facilities to meet its long term exploration goals.[1] In particular, self-pressurization of these tanks in 1g and microgravity has been the subject of several recent numerical[2–4] and experimental[5,6] studies. These investigations have focused on elucidating the complicated transport issues that arise when

*21000 Brookpark Rd., MS:110-3, Cleveland, OH 44135

a cryogenic storage tank is subjected to a heat leak from the surrounding environment. The heat leak can arise from a variety of sources including solar radiation, aerodynamic heating, and conduction through the tank's support structure. When heat enters the tank, natural convection currents carry this thermal energy to the liquid vapor interface. As the warmer fluid reaches the interface, evaporation will occur resulting in vapor compression and a subsequent rise in tank pressure. Predicting the boil-off rate, and thus the self-pressurization rate, for a variety of heat loads, distributions, and engineering specifications, is not only important from a structural standpoint but also for designing tank pressure control systems.

To meet this need in the engineering community, a number of numerical models have been developed that predict the pressurization behavior of a cryogenic storage tank subject to some external heat load. The lowest order model that can be used to predict the self-pressurization rate is a homogeneous thermodynamic model.[2,5,7] This lumped formulation applies the first law of thermodynamics to a cryogenic tank and thus assumes homogeneity in the system. That is; the liquid and vapor phases can be represented by a single thermodynamic state with a common pressure and temperature. Unfortunately, application of these simple models have resulted in discrepancies between the measured and predicted vapor pressure levels. The source of these discrepancies is often attributed to initial transient transport driven by natural convection thermal boundary layers that develop along the tank's walls.

To resolve this shortcoming, numerical models have been developed which integrate the conservation equations across the natural convection boundary layer.[8] These models assume a well-defined form of the thermal and momentum boundary layers, which in reality may not exist in complicated tank geometries and heating configurations. To address this limitation, Panzarella and Kassemi[2] developed a two-phase lumped vapor active liquid model that couples the evolution of ullage pressure, predicted by a lumped thermodynamic model of the vapor, to the detailed solution of the Navier-Stokes and energy equations for flow and heat transfer in the liquid.

In this paper, both a homogeneous thermodynamic model and a two-phase lumped vapor CFD model will be presented, described, and used to investigate the self-pressurization behavior of a flightweight LH2 tank prototype in 1g. Model predictions will be discussed and compared against pre-existing cryogenic self-pressurization data gathered during experiments in NASA Glenn's K-site facility.

II. Experimental Description

The pressurization tests examined here were conducted using the flightweight LH2 tank in the K-site facility at NASA Glenn's Plum Brook Station.[6,9,10] The facility consisted of a vacuum chamber enclosing a cylindrical cryoshroud whose temperatures can be maintained with electrical resistance heaters. Within the shroud, an LH2 tank was suspended by twelve fiberglass composite struts. The tank was constructed of 2219 aluminum with a wall thickness varying between 1.9558×10^{-3} m and 2.2098×10^{-3} m. The tank was fabricated by joining two halves of a 1.2/1 oblate spheroid to a 0.0381 m cylindrical section. The major and minor diameters of the oblate spheroid were 2.22504 m and 1.8542 m, respectively. The internal tank volume was 4.955 m^3. The tank was covered by two MLI blankets to reduce radiative losses.

Before the self-pressurization experiments began, boil-off tests were performed to estimate the net heat leak into the LH2 tank. During these tests, the tank was 95% full of LH2 and the operating pressure was approximately 117 kPa. Heat leak into the tank caused the liquid to evaporate and the resulting boil-off was directed through volume flow meters. For the lower heat flux cases, a steady boil-off rate of 2.7 SCMH was recorded. From this boil-off rate, the net heat power into the system was determined to be 30.01 W. Once this steady boil-off rate was determined, the tank was drained to the desired fill level, the operating pressure was reduced to 103 kPa, and venting occurred for another four hours before tank lock-up. Finally lock-up occurred and the tank was allowed to self-pressurize for approximately 20 hours.

III. Mathematical Formulation

A. Thermodynamic Model

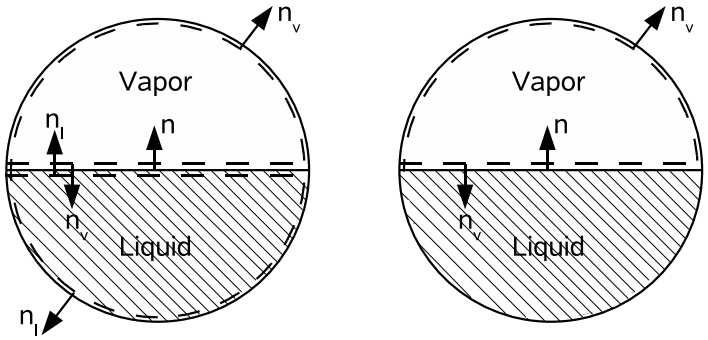

(a) (b)

Figure 1. Partially filled tank in 1g with (a) two control volumes bounding each phase for the thermodynamic analysis and (b) one control volume bounding the vapor phase for the lumped vapor analysis.

Consider a tank partially filled with liquid as shown in Fig. 1. We can define two control volumes bounding the liquid and vapor phases. If we neglect viscous dissipation and integrate the energy conservation equation over each control volume, we get:

$$\frac{d}{dt}\int \rho_v e_v dV + \int \rho_v e_v(\mathbf{v}-\mathbf{v_s})\cdot\hat{n}_v dS = -\int \mathbf{q_v}\cdot\hat{n}_v dS - \int p\nabla\cdot\mathbf{v}dV \tag{1}$$

$$\frac{d}{dt}\int \rho_l e_l dV + \int \rho_l e_l(\mathbf{v}-\mathbf{v_s})\cdot\hat{n}_l dS = -\int \mathbf{q_l}\cdot\hat{n}_l dS - \int p\nabla\cdot\mathbf{v}dV \tag{2}$$

The surface integrals can be broken into integrals along the tank wall and integrals over the interface while noting that along the wall, the convective contribution is zero and along the interface $\hat{n} = \hat{n}_l = -\hat{n}_v$.

$$\frac{d}{dt}\int \rho_v e_v dV - \int_I \rho_v e_v(\mathbf{v}-\mathbf{v_s})\cdot\hat{n}dS = -\int_w \mathbf{q_v}\cdot\hat{n}_v dS + \int_I \mathbf{q_v}\cdot\hat{n}dS - \int p\nabla\cdot\mathbf{v}dV \tag{3}$$

$$\frac{d}{dt}\int \rho_l e_l dV + \int_I \rho_l e_l(\mathbf{v}-\mathbf{v_s})\cdot\hat{n}dS = -\int_w \mathbf{q_l}\cdot\hat{n}_l dS - \int_I \mathbf{q_l}\cdot\hat{n}dS - \int p\nabla\cdot\mathbf{v}dV \tag{4}$$

We now decompose the pressure field into a mean field and a variation around the mean:

$$p = \overline{p}\left(1+\frac{p'}{\overline{p}}\right) \tag{5}$$

If we further assume that the variation is small compared to the mean

$$p \approx \overline{p} \tag{6}$$

the last terms in equations (3) and (4) can be rewritten as:

$$-\int p\nabla\cdot\mathbf{v}dV \approx -\overline{p}\int_I \mathbf{v}\cdot\hat{n}dS \tag{7}$$

$$= -\overline{p}\int_I (\mathbf{v}-\mathbf{v_s})\cdot\hat{n}dS - \overline{p}\int_I \mathbf{v_s}\cdot\hat{n}dS \tag{8}$$

$$= -\overline{p}\int_I (\mathbf{v}-\mathbf{v_s})\cdot\hat{n}dS - \overline{p}\frac{dV}{dt} \tag{9}$$

This leads to:

$$\frac{d}{dt}\int \rho_v e_v dV - \int_I \rho_v e_v(\mathbf{v}-\mathbf{v_s})\cdot\hat{n}dS = -\int_w \mathbf{q_v}\cdot\hat{n}_v dS + \int_I \mathbf{q_v}\cdot\hat{n}dS + \overline{p}\int_I(\mathbf{v_v}-\mathbf{v_s})\cdot\hat{n}dS - \overline{p}\frac{dV_v}{dt} \quad (10)$$

$$\frac{d}{dt}\int \rho_l e_l dV + \int_I \rho_l e_l(\mathbf{v}-\mathbf{v_s})\cdot\hat{n}dS = -\int_w \mathbf{q_l}\cdot\hat{n}_l dS - \int_I \mathbf{q_l}\cdot\hat{n}dS - \overline{p}\int_I(\mathbf{v_l}-\mathbf{v_s})\cdot\hat{n}dS - \overline{p}\frac{dV_l}{dt} \quad (11)$$

We now assume that ρ and e are constant along either side of the interface. The above two equations can thus be rewritten:

$$\frac{d}{dt}\int \rho_v e_v dV - e_v\int_I \rho_v(\mathbf{v}-\mathbf{v_s})\cdot\hat{n}dS = \dot{Q}_{wv} + \dot{Q}_{iv} + \frac{\overline{p}}{\rho_v}\int_I \rho_v(\mathbf{v_v}-\mathbf{v_s})\cdot\hat{n}dS - \overline{p}\frac{dV_v}{dt} \quad (12)$$

$$\frac{d}{dt}\int \rho_l e_l dV + e_l\int_I \rho_l(\mathbf{v}-\mathbf{v_s})\cdot\hat{n}dS = \dot{Q}_{wl} - \dot{Q}_{il} - \frac{\overline{p}}{\rho_l}\int_I \rho_l(\mathbf{v_l}-\mathbf{v_s})\cdot\hat{n}dS - \overline{p}\frac{dV_l}{dt} \quad (13)$$

where we have defined:

$$\dot{Q}_{wv} = -\int_w \mathbf{q_v}\cdot\hat{n}_v dS \quad (14)$$

$$\dot{Q}_{wl} = -\int_w \mathbf{q_l}\cdot\hat{n}_l dS \quad (15)$$

$$\dot{Q}_{iv} = \int_I \mathbf{q_v}\cdot\hat{n}dS \quad (16)$$

$$\dot{Q}_{il} = \int_I \mathbf{q_l}\cdot\hat{n}dS \quad (17)$$

Defining M to be the integrated form of mass flux jump condition:

$$M = \int_I \rho_v(\mathbf{v_v}-\mathbf{v_s})\cdot\hat{n}dS = \int_I \rho_l(\mathbf{v_l}-\mathbf{v_s})\cdot\hat{n}dS \quad (18)$$

and adding eqns. (12) and (13) yields:

$$\frac{d}{dt}\left[\int \rho_v e_v dV + \int \rho_l e_l dV\right] - M(e_v - e_l) = \dot{Q}_w + \dot{Q}_{iv} - \dot{Q}_{il} + \overline{p}M\left(\frac{1}{\rho_v} - \frac{1}{\rho_l}\right) \quad (19)$$

where $\dot{Q}_w$ is the net heat entering the system through the wall. We have also made use of the fact that the tank is rigid:

$$\frac{dV_T}{dt} = \frac{d}{dt}(V_l + V_v) = 0 \quad (20)$$

To simplify equation (19) we note that at equilibrium:

$$e_v - e_l = L - \overline{p}\left(\frac{1}{\rho_v} - \frac{1}{\rho_l}\right) \quad (21)$$

We can also employ the integrated form of the energy jump condition:

$$LM = \dot{Q}_{il} - \dot{Q}_{iv} \quad (22)$$

After substituting eqns. (21) and (22) into equation (19), several terms cancel leading to:

$$\frac{d}{dt}\left[\overline{\rho_v e_v}V_v + \overline{\rho_l e_l}V_l\right] = \dot{Q}_w \quad (23)$$

where the overbars denote averages over the respective control volumes. We can now invoke the homogeneous approximation:

$$\overline{\rho_v e_v} = \rho_v e_v = \rho_s e_s \quad (24)$$

$$\overline{\rho_l e_l} = \rho_l e_l \quad (25)$$

where the subscript s denotes the saturation state and it is assumed that both phases share the common temperature T_s. Thus we have

$$\frac{d}{dt}\left[\rho_s e_s V_v + \rho_l e_l V_l\right] = \dot{Q}_w \tag{26}$$

The above equation can be simplified by substituting appropriate expressions for density, internal energy, and vapor volume and carrying out the differentiation. The full derivation has been presented elsewhere[2, 11] and results in a pressure evolution equation of the form

$$\boxed{\frac{dp_s}{dt}\left\{(\rho_s c_v V_v + \rho_l c_l V_l)\frac{dT_s}{dp_s} + \frac{\partial(\rho_s V_v)}{\partial p_s}\left[L - p_s\left(\frac{1}{\rho_s} - \frac{1}{\rho_l}\right)\right]\right\} = \dot{Q}_w} \tag{27}$$

This evolution equation is implicit in p_s since

$$\rho_s(p_s) = \frac{p_s}{RT_s(p_s)} \tag{28}$$

$$V(\rho_s(p_s)) = V^o\frac{\rho_l - \rho_s^o}{\rho_l - \rho_s(p_s)} \tag{29}$$

$$T_s(p_s) = \left(\frac{1}{T_B} - \frac{R}{L}\ln\frac{p_s}{p_B}\right) \tag{30}$$

Equation (29) is a consequence of integrating in time the integral form of continuity. The superscript o in eq. (29) denotes in the initial vapor state. Equation (30) is the Clausius-Clapeyron equation, an equilibrium saturation condition relating the saturation pressure to the saturation temperature.

The rigorous derivation above precisely defines all the assumptions invoked in deriving the homogeneous thermodynamic model and thus sets the necessary conditions to get agreement between the thermodynamic predictions and the experimental measurements. To summarize, we should expect agreement between the thermodynamic model and the experiment when the average energy of the system changes at the same rate as the system energy defined by the saturation state – a condition typically met after all system transients have decayed and a stationary state has been established. The assumptions required to reach this conclusion are:

1. Volumetric energy sources other than compressibility effects (e.g., viscous dissipation, ortho/para conversion) are negligible.

2. Variations in ullage pressure around the saturation pressure can be neglected.

3. Density and internal energy are constant along either side of the interface.

4. Interfacial mass transfer is sufficiently small for terms $\dot{M}^2$ and higher to be negligible in the interfacial energy jump equation.

Several additional assumptions (e.g., ideal gas behavior, constant liquid density) have also been invoked to transform the thermodynamic energy balance into the thermodynamic pressure evolution equation. These simplifying assumptions only serve to make the analysis more tractable, are not central to the conclusions reached thus far, and can oftentimes be relaxed.

B. Lumped Vapor Active Liquid CFD Model

As previously mentioned, thermodynamics is able to predict the pressurization rate after all system transients have decayed. To capture these transients, and better resolve the pressurization behavior, more sophisticated models are required. Generally, the time constants associated with transport in the liquid are much longer than the corresponding time scales in the vapor region. Consequently, we follow the approach of Panzarella and Kassemi[2] and couple the detailed transport equations in the liquid to a lumped energy and mass model of the vapor. The two-phase lumped vapor pressure evolution equation is derived by proceeding similarly as

before. First a control volume bounding the vapor phase is defined as shown in Fig. 1b. Integral energy and mass balances are performed, which after invoking the same simplifying assumptions listed earlier leads to

$$\boxed{\frac{dp_s}{dt}\left\{\rho_s c_v V_v \frac{T_s}{dp_s} + \frac{\partial(\rho_s V_v)}{\partial p_s}\left[L - p_s\left(\frac{1}{\rho_s} - \frac{1}{\rho_l}\right)\right]\right\} = \dot{Q}_{wv} + \dot{Q}_{il}} \tag{31}$$

This evolution equation for ullage pressure is coupled to the transport equations in the liquid by $\dot{Q}_{il}$, the integrated heat flux on the liquid side of the interface, which is computed explicitly from the computed spatial temperature distributions in the liquid phase.

In the liquid region the incompressible, axisymmetric, Reynolds averaged continuity, Navier-Stokes, and energy conservation equations are solved along with Menter's shear stress transport $k-\omega$ turbulence equations.[12] Of the various two-equation turbulence models available, prior benchmarking by the authors have revealed that Menter's SST model is most suitable for the current cryogenic tank problem. In the conservation equations in the liquid, all properties are assumed constant except density To account for small density variations, the Boussinesq approximation is applied to the body force term in the axial momentum equation. Relevant thermophysical properties used in both the thermodynamic and lumped vapor formulations are listed in Table 1.

Table 1. Relevant Saturation Properties at 20.333 K[13]

Parameter	Value
ρ_l	70.734 kg/m^3
c_l	5678.2 J/kg K
k_l	0.10349 W/m K
μ_l	$1.324{\cdot}10^{-5}$ kg/m s
β	0.0168 K^{-1}
M	0.00201594 kg/mol
L	445196.6 J/kg
c_v	6605.4 J/kg K

Along the symmetry axis, Neumann conditions on temperature, velocity, turbulence variables are defined. Along the wetted-wall, a prescribed uniformly distributed heat flux of 2.13 W/m^2 is imposed. Additionally, no-slip conditions and enhanced wall function treatment are used as boundary conditions for the flow and turbulence equations. To simplify the computational analysis, the interface is treated as a stationary slip wall with a prescribed temperature set equal to the saturation temperature corresponding the pressure in the vapor region. Thus, the interfacial temperature couples the solution in the liquid region to the pressure evolution equation for the ullage through the dependancy of T_s on p_s. The kinematic constraint is also enforced on the surface which is a reasonable approximation for a stationary interface in the limit of $\dot{M} << 1$.

IV. Numerical Implementation

The lumped vapor model has been implemented into the commercial CFD code Fluent. The underlying code solves the continuity, Navier-Stokes, energy conservation, and turbulence equations in the liquid. The interfacial mass transfer model and vapor pressure updating scheme is implemented via customized user-defined functions.

In the liquid the flow, energy, and turbulence equations are evolved in time using a first order backward Euler scheme with a fixed time-step of 0.9 seconds. Spatially, in the momentum and energy equations, a 3rd order monotone upwinding scheme is used to discretize the convective fluxes. In the turbulence equations, 2nd order upwinding is applied. SIMPLE pressure-velocity coupling is used to enforce continuity. The results shown herein were generated on a non-orthogonal mesh of approximately 10000 quadrilateral control volumes with a dense clustering of cells near the tank wall and liquid-vapor interface to resolve the turbulent natural

convection boundary layer and interfacial heat fluxes, respectively. The equations are solved sequentially using the standard parallel algebraic multigrid solver with a Gauss-Seidel smoother. Convergence is attained within each time step when the L1 norm of the residual for all the primary variables falls below 1×10^{-6}. It takes approximately 4 days of CPU time on 6 AMD 64 bit Opteron processors to simulate the 20 hour experiment.

The interface is modeled as a stationary slip boundary with a prescribed temperature set equal to the saturation temperature corresponding to the pressure in the ullage. Within each outer iteration, the interfacial heat power on the liquid side of the interface is computed and used to update the vapor pressure according to Eq. (31). This non-linear evolution equation is updated using Newton-Raphson iteration. Once the vapor pressure is updated, a new saturation temperature is computed and prescribed on the slip boundary of the computational domain.

In validating a model or code against experimental data, the correct representation of the experimental boundary and initial conditions is crucial. In the present validation process, due to a lack of more detailed spatial experimental data, we are forced to assume that the net heat load is uniformly distributed around the tank. This corresponds to a heat flux of 2.13 W/m^2 that is imposed as a boundary condition on the wall-liquid boundary in the numerical model. The remaining heat power $\dot{Q}_{wv} = 30.01 - 2.13\,A_l$ is entered directly into the pressure evolution equation. In the above expression, A_l, the wetted wall area varies depending on the liquid fill level. Hence, for the cases studied here, while the net heat load is the same for the different fill levels, because the wetted wall area is changing, the partitioning of the heat load into the two phases is also varying.

Experimentally, prior to self-pressurization, during an initialization period the tank is vented for several hours at an operating pressure of 103 kPa. To have an initial condition for the self-pressurization simulations, steady-state flow and temperature fields are obtained during the venting period and used as the initial input for the self-pressurization runs. During the steady-state simulations of the initialization period, the interfacial temperature is fixed and set equal to the saturation temperature corresponding to 103 kPa. It may seem contrived to obtain a steady-state solution during venting when in reality no steady solution should physically exist. That is, during venting liquid is being consumed, therefore the interface is receding into the liquid, and energy is being consumed as phase change takes place – all of which imply that the conditions are not steady. By using the steady-state solution to represent the venting period, all of the above mentioned effects have been judged to be negligible.

Indeed the steady-state behavior may not be far from reality. To see this more clearly, consider that during the boil-off tests, the mass flow out of the tank was measured:

$$\dot{M}_{out} = 2.7 \text{ SCMH} = 6.74 \times 10^{-5}\text{kg/s}$$

Applying the integral form of continuity to a control volume bounding the vapor region, one can relate the mass flux out of the tank to the interfacial mass flux. Assuming an incompressible liquid and homogenous liquid and vapor regions,

$$\dot{M}\left(1 - \frac{\rho_s}{\rho_l}\right) = \dot{M}_{out}$$

Thus, at a pressure of 103 kPa, $T_s = 20.333K$ and $\dot{M} = 6.87 \times 10^{-5}$ kg/s. Once again, from the integral form of continuity, it can be shown that the time rate of change of vapor volume during these boil-off tests is:

$$\frac{dV}{dt} = \frac{\dot{M}}{\rho_l}$$

Using the values computed above, $\frac{dV}{dt} = 9.7 \times 10^{-7}\frac{m^3}{s}$. At the 29% and 49% fill levels, the interfacial area is 3.59 m^2 and 3.89 m^2, respectively. Thus, the maximum rate the interface is receding into the liquid is 2.70×10^{-7} m/s, which is not practically resolvable over of the time scale of the initialization period.

The interfacial heat power during the steady boil-off process can be determined by performing an integral energy balance over the liquid region. Assuming constant liquid density:

$$\dot{Q}_{il} = \dot{Q}_{wl} - \dot{M}(e_s - \overline{e}_l)$$

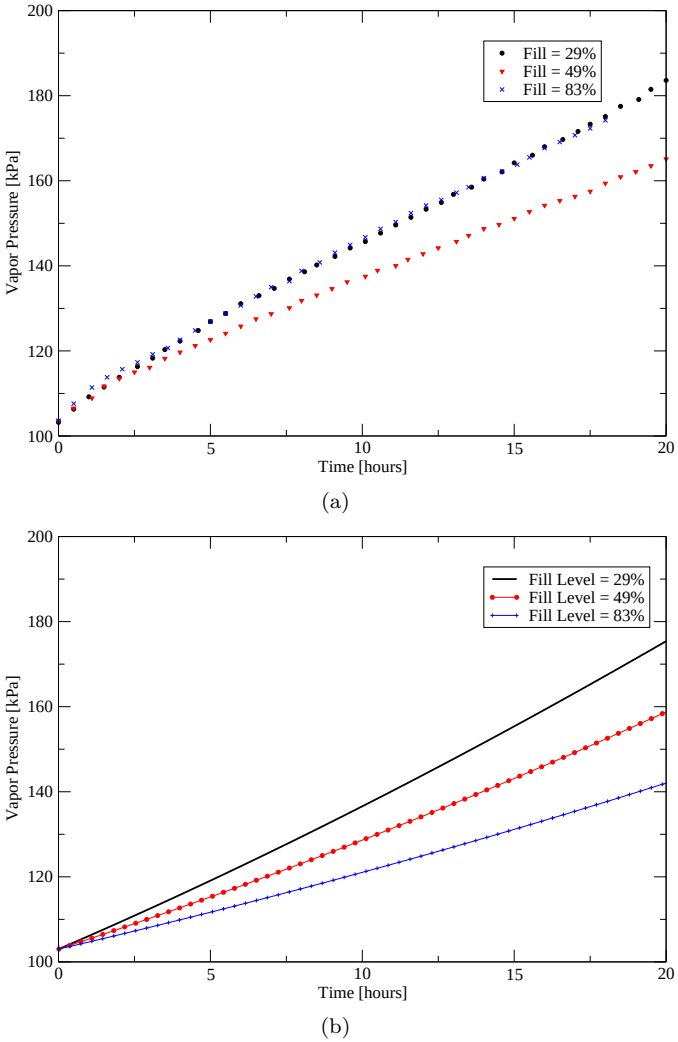

Figure 2. Vapor pressure histories for three different fill levels. (a) Experimental data (Ref 6). (b) Thermodynamics.

Because a steady-state solution enforces $\dot{Q}_{il} = \dot{Q}_{wl}$, the second term on the right side of the above expression can be thought of as the error associated with initializing the self-pressurization cases using a steady-state analysis. To estimate the magnitude of this error, analysis of the steady-state computational results reveal that the average bulk liquid temperature is 20.387 K and 20.411 K for the 29% and 49% cases, respectively. As expected, the average bulk liquid temperature is reduced for the lower fill level case. For the lower fill level, because of the smaller wetted-wall area, less energy is entering the liquid region. The error can be estimated by $\dot{M}c_l|T_s - \overline{T}|$ which evaluates to 0.02 W for the 29% fill case and 0.03 W for the 49% fill cases. This error in the interfacial heat power has a negligible effect on the overall heat balance and once again, performing a steady-state analysis to initialize the solution appears to be justified.

V. Discussion

Experimental vapor pressure histories are shown in Fig. 2a for the three different liquid fill levels. These data sets correspond to the lower heat flux cases (2.13 W/m^2) studied in the experiment. It is difficult to interpret the effect of liquid fill level on the self-pressurization rate based solely on the experimental data. Data for the 29% and 83% cases indicate that no trend exists which is quite contrary to the thermodynamic predictions of how the system should respond for a given heat load. As shown in Fig. 2b, thermodynamics predicts that the pressurization rate decreases with increasing fill level. This result is intuitive since the dom-

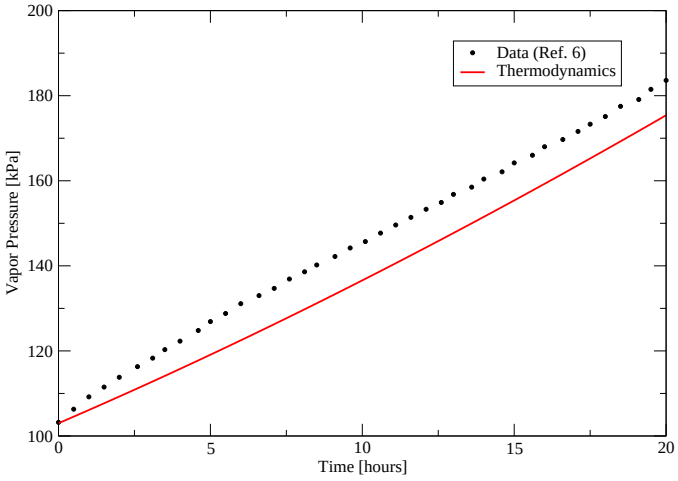

(a)

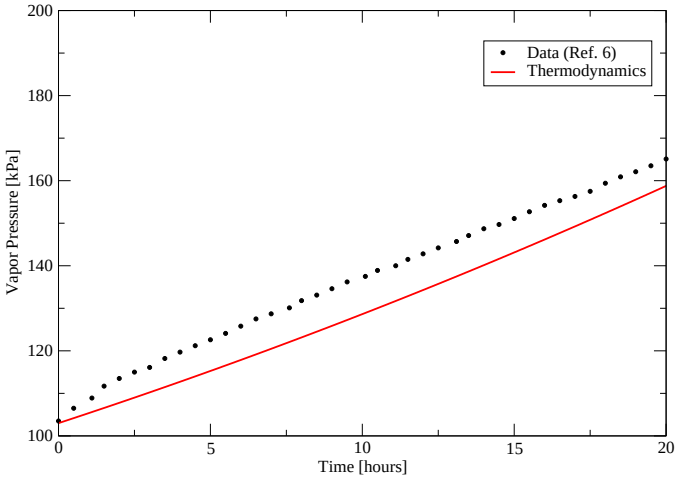

(b)

Figure 3. Comparisons between thermodynamics and experimental data. (a) Fill level = 29%. (b) Fill level = 49%

inant term in the thermodynamic evolution equation for the cases studied here is $\rho_l\, c_l\, V_l\, \frac{dT_s}{dp_s}$ which represents changes in the internal energy of the liquid. Thus, as liquid volume increases, because of increasing fill level, the self-pressurization rate should be reduced. Given this crucial discrepancy between thermodynamics and experimental data, one may question whether or not the data should even agree with the thermodynamic predictions. Indeed, discrepancies between thermodynamics and experimental data are often left unexplained and usually misattributed to thermal stratification in the vapor.[6,14] Rigorous analysis presented earlier in this paper demonstrates that the long-term pressurization rate is captured by thermodynamics which predicts a decreased pressurization rate for increasing fill levels. Because this trend is correctly exhibited in the 29% and 49% data sets, subsequent discussion will be limited to these cases. A more thorough review of the experimental data for the 83% case is needed and will be considered in the near future.

Comparisons between the experimental data and thermodynamics are shown in Fig. 3. Clearly, thermodynamics does an excellent job of predicting the rate of self-pressurization but does not capture the actual level of the vapor pressure. The pressure level is greatly affected by initial transient transport in the liquid and the thermodynamic analysis is unable to capture any transients in the system.

To overcome the shortcoming of the thermodynamic model, we decided to model the transport in the liquid based on a full Navier-Stokes and conservation of energy analysis for the fluid flow and heat transfer

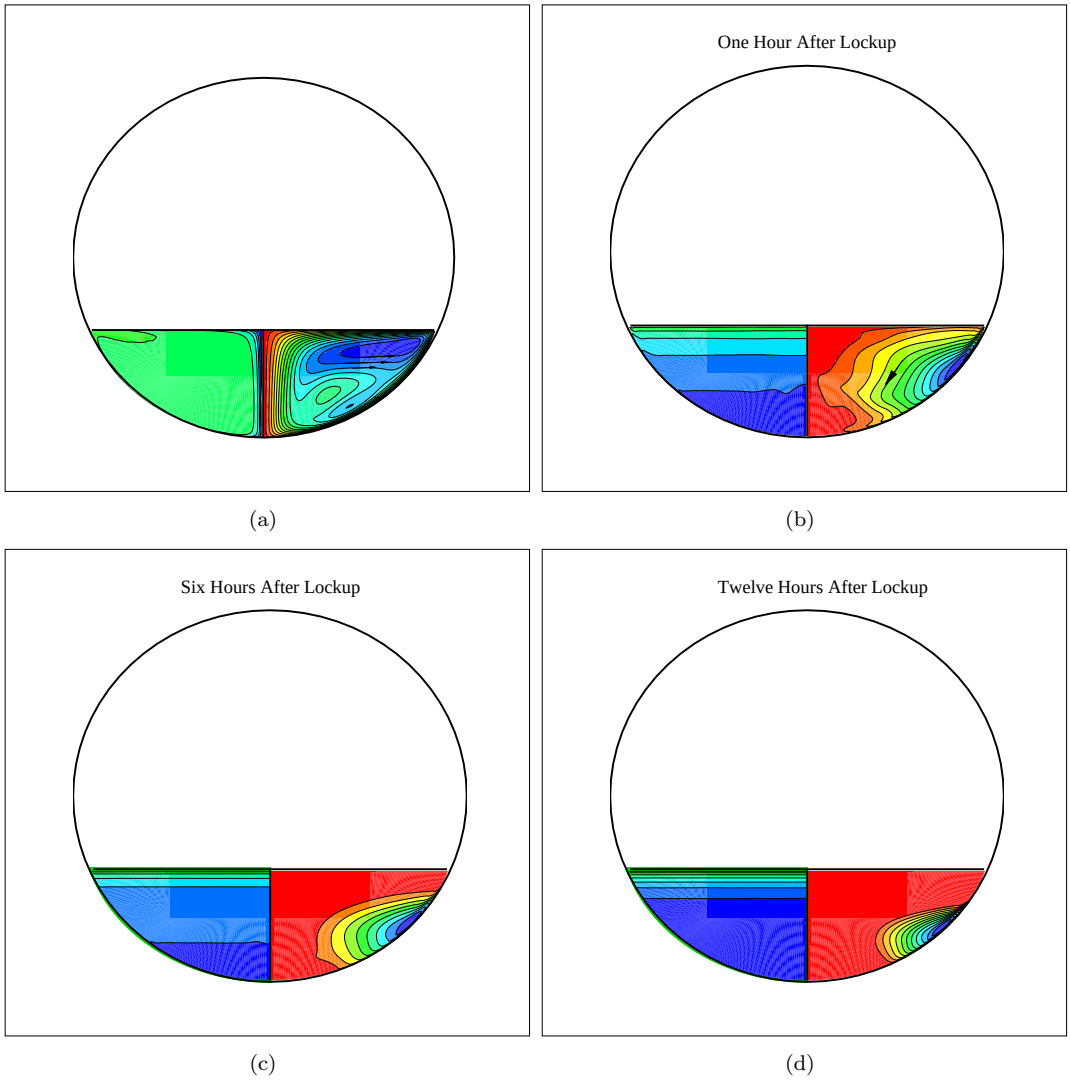

Figure 4. Isocontours of temperature and stream function during self-pressurization (Fill Level = 29%)

in the liquid. Because the time scales associated with transport in the vapor are typically much faster than the corresponding time scales in the liquid, we decided that a lumped analysis of the vapor is adequate and coupled it to the detailed transport analysis in the liquid. The resulting two-phase lumped vapor active liquid CFD model can thus resolve any transient phenomena that might develop in the liquid.

The temperature and flow field solution for the 29% fill case is shown in Fig. 4. To conserve space in this and subsequent contour plots, isocontours of temperature are shown in the left of each figure while isocontours of the stream function field are shown in the right. The initial fields to the self-pressurization simulation is shown in Fig. 4a with subsequent snapshots in time given in Figs. 4b-d. Initially, strong turbulent natural convection in the liquid results in a well-mixed thermal field. The liquid is essentially isothermal save for thin regions along the tank wall, the symmetry axis, and the interface. During this time, the bulk temperature of the liquid is limited by the interfacial temperature which is fixed to 20.333 K. Once self-pressurization is allowed to take place, the interfacial temperature can vary in response to changes in vapor pressure. Owing to a uniform heating distribution, once tank lock-up occurs, a significant amount of heat is being added directly into the vapor. Consequently, the interfacial temperature is rising faster than the bulk liquid temperature which creates a stably stratified liquid thus reducing the strength of the natural convection below the interface as seen in the time progression shown in Figs. 4b-d. Similar behavior is observed for the 49% fill case shown in Fig. 5.

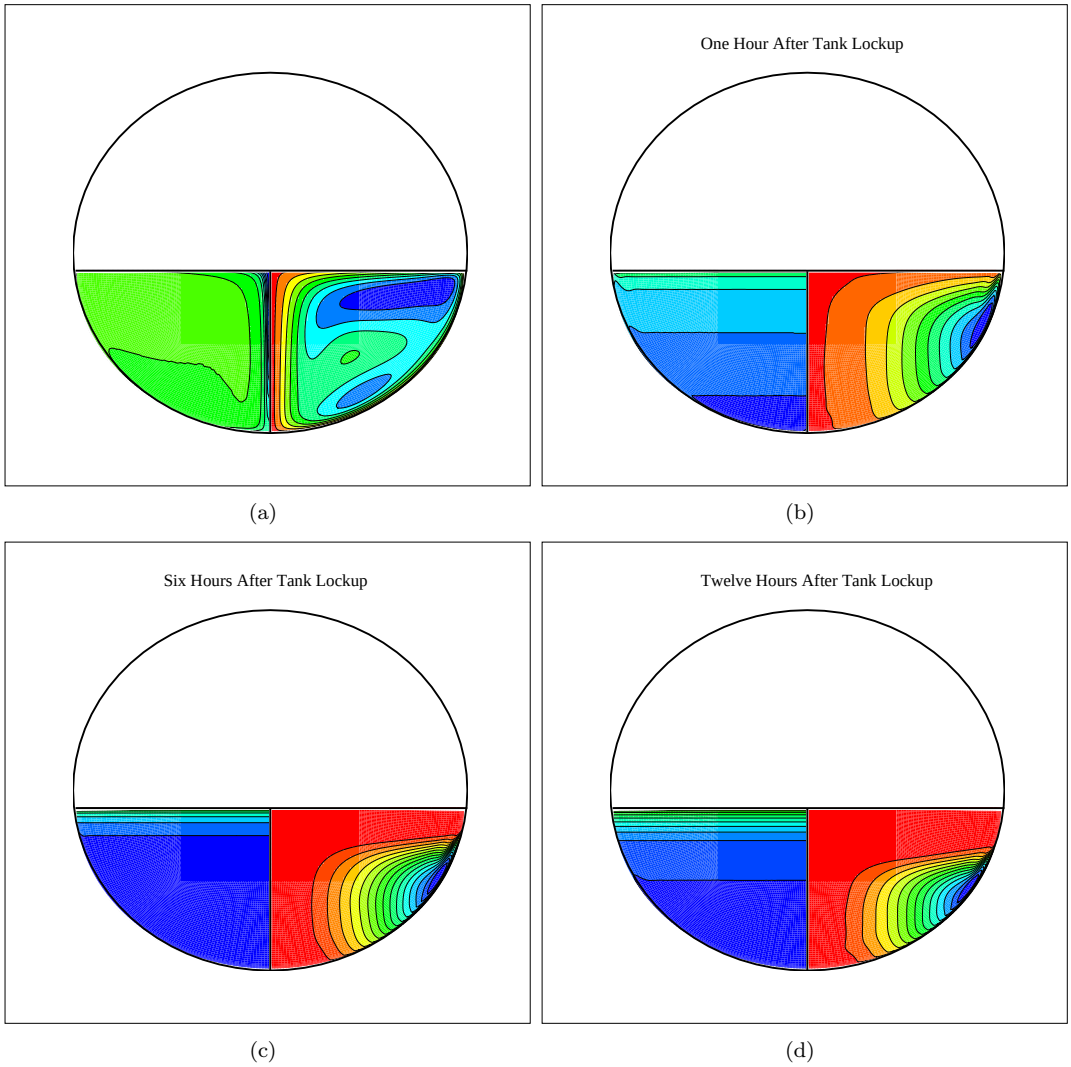

Figure 5. Isocontours of temperature and stream function during self-pressurization (Fill Level = 49%)

Comparisons between the vapor pressure history predicted by the two-phase lumped vapor CFD model and the experimental data are shown in Fig. 6 for the 29% fill case and in Fig. 7 for the 49% fill case. As the comparisons for the 29% case clearly indicate, the lumped vapor model does an excellent job of predicting both the self-pressurization rate and the magnitude of the vapor pressure. However, for the 49% fill case, a slight discrepancy exists. While the pressurization rate is accurately captured, the magnitude of the vapor pressure rise is overpredicted. Possible sources for this discrepancy may include temperature dependant properties in the liquid, real fluid effects in both the liquid and vapor, or non-representative boundary/initial conditions. To underscore the sensitivity of the results to the heat flux boundary condition, in Fig. 7, we have included the vapor pressure history assuming that the entire heat load enters the system through the wetted wall. Clearly, the data is bounded by the uniform and liquid-only heating configurations suggesting a non-uniform heat distribution may be responsible for the discrepancy between the predicted and measured pressure histories. Conduction paths through the tank support struts in the liquid region may be the cause of the heat load non-uniformity. However further examination is required to judge whether or not this is actually the case.

While the results presented thus far would seem to suggest that the homogeneous thermodynamic model can accurately predict the rate of self-pressurization and the two-phase lumped vapor active liquid CFD

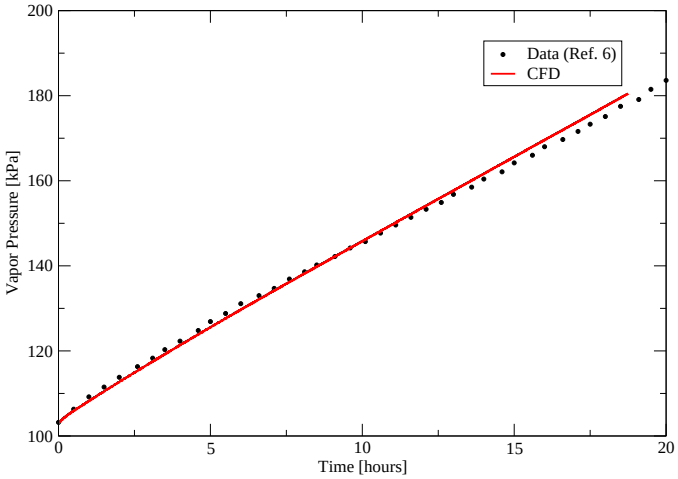

Figure 6. Comparison between CFD and experimental data (Fill Level = 29%)

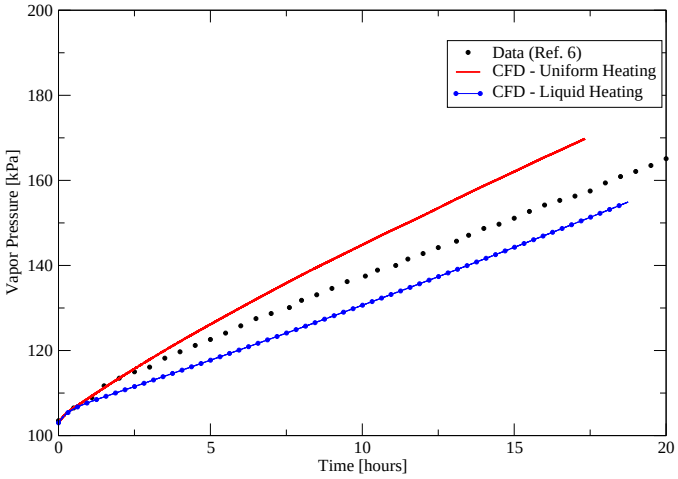

Figure 7. Comparison between CFD and experimental data (Fill Level = 49%)

model does a reasonable job of predicting both the magnitude of the vapor pressure and the pressurization rate, we feel additional analysis is still required before the aforementioned models can be considered truly validated. In attempting to explain the discrepancy shown in Fig. 7, the thermodynamic energy balance (eq. (26)) was solved directly instead of making the simplifying assumptions associated with the evolution equation (eq. (27)) previously described. Solution of this more complete energy balance resulted in a slight underprediction of the self-pressurization rate. A more detailed analysis is currently underway and results will be presented in future publications.

VI. Conclusions

In this paper, a homogeneous thermodynamic model and a two-phase lumped-vapor CFD model were developed and presented to describe the self-pressurization behavior of a flightweight partially filled LH2 tank in normal gravity. Existing experimental data was used to assess the predictive capability of these models. Comparisons between the data and the model predictions indicate that the homogeneous thermodynamic model can accurately predict the self-pressurization rate, but fails to capture the magnitude of the pressure rise. This shortcoming is primarily due to the inability of the thermodynamic model to capture the initial transient transport in the tank. To address this shortcoming, a two-phase lumped vapor model is coupled

to the detailed Navier-Stokes and energy transport equations in the liquid. This lumped vapor active liquid CFD model correctly predicts both the pressurization rate and the magnitude of ullage pressure levels for the lower fill cases measured experimentally. For higher fill levels, some discrepancies between the numerical predications and the experimental data are observed. Uncertainty in the experimental heating distribution has been suggested as a likely cause of this discrepancy.

References

[1]F. P. Chiaramonte and J. A. Joshi. Workshop on critical issues in microgravity fluids, transport, and reaction processes in advanced human support technology: Final report. NASA TM 2004-212940, 2004.

[2]C. H. Panzarella and M. Kassemi. On the validity of purely thermodynamic descriptions of two phase cryogenic fluid storage. *J. Fluid Mech.*, 484:41–68, 2003.

[3]C. H. Panzarella and M. Kassemi. Self-pressurization of large spherical cryogenic tanks in space. *J. Spacecraft and Rockets*, 42(2):299–308, 2005.

[4]C. Panzarella, D. Plachta, and M. Kassemi. Pressure control of large cryogenic tanks in microgravity. *Cryogenics*, 44:475–483, 2004.

[5]J. C. Aydelott. Effect of gravity on self-pressurization of spherical liquid hydrogen tankage. NASA TN D-4286, 1967.

[6]N. T. VanDresar, C. S. Lin, and M. M. Hasan. Self-pressurization of a flightweight liquid hydrogen tank: Effects of fill level at low wall heat flux. NASA TM 105411, 1992.

[7]C. S. Lin, N. T. VanDresar, and M. M. Hasan. Pressure control analysis of cryogenic storage systems. *J. Propulsion and Power*, 20(3):480–485, 2004.

[8]R. W. Arnett and R. O. Voth. A computer program for the calculation of thermal stratification and self-pressurization in a liquid hydrogen tank. NASA CR 2026, 1972.

[9]R.J. Stochl and R.H. Knoll. Thermal performance of a liquid hydrogen tank multilayer insulation system at warm boundary temperatures of 630, 530 and 152 r. NASA TM 104476, 1991.

[10]M. M. Hasan, C. S. Lin, and N.T. Van Dresar. Self-pressurization of a flightweight liquid hydrogen storage tank subjected to a low heat flux. NASA TM 103804, 1991.

[11]S. Barsi, M. Kassemi, C.H. Panzarella, and J.I.D. Alexander. A tank self-pressurization experiment using a model fluid in normal gravity. AIAA2005-1143, 2005.

[12]F.R. Menter, M. Kuntz, and R. Langtry. Ten years of experience with the sst turbulence model. In K. Hanjalic, Y. Nagano, and M. Tummers, editors, *Turbulence, Heat and Mass Transfer 4*, pages 625–632. Begell House Inc., 2003.

[13]P.J. Linstrom and W.G. Mallard, editors. *NIST Chemistry WebBook, NIST Std. Ref. Database Number 69*. NIST, 2005. http://webbook.nist.gov.

[14]N.V. Amirkhanyan and S.G. Cherkasov. Theoretical analysis and procedure for the calculation of thermophysical processes occurring in a cryogenic vessel under conditions of nonvented storage. *High Temperature*, 39(6):905–911, 2001.